Cell

Prdm3 and Prdm16 are H3K9me1 Methyltransferases Required for Mammalian Heterochromatin Integrity

Inês Pinheiro,[1,2] Raphaël Margueron,[3,6] Nicholas Shukeir,[1] Michael Eisold,[1] Christoph Fritzsch,[1] Florian M. Richter,[1] Gerhard Mittler,[1] Christel Genoud,[4] Susumu Goyama,[5,7] Mineo Kurokawa,[5] Jinsook Son,[3] Danny Reinberg,[3] Monika Lachner,[1] and Thomas Jenuwein[1,2,*]

[1]Department of Epigenetics, Max Planck Institute of Immunobiology and Epigenetics, Stübeweg 51, 79108 Freiburg, Germany
[2]Research Institute of Molecular Pathology, Dr. Bohrgasse 7, 1030 Vienna, Austria
[3]Department of Biochemistry, New York University School of Medicine-Smilow Research Center, 522 First Avenue, New York, NY 10016, USA
[4]Friedrich Miescher Institute for Biomedical Research, Maulbeerstrasse 66, 4058 Basel, Switzerland
[5]Department of Hematology and Oncology, The University of Tokyo Hospital, 7-3-1 Hongo, Bunkyo-ku, Tokyo 113-8655, Japan
[6]Present address: Institut Curie, 11-13 Rue Pierre et Marie Curie, 75005 Paris, France
[7]Present address: Division of Experimental Hematology and Cancer Biology, Cincinnati Children's Hospital Medical Center, Cincinnati, OH 45229, USA
*Correspondence: jenuwein@ie-freiburg.mpg.de
http://dx.doi.org/10.1016/j.cell.2012.06.048

SUMMARY

Heterochromatin serves important functions, protecting genome integrity and stabilizing gene expression programs. Although the Suv39h methyltransferases (KMTs) are known to ensure pericentric H3K9me3 methylation, the mechanisms that initiate and maintain mammalian heterochromatin organization remain elusive. We developed a biochemical assay and used in vivo analyses in mouse embryonic fibroblasts to identify Prdm3 and Prdm16 as redundant H3K9me1-specific KMTs that direct cytoplasmic H3K9me1 methylation. The H3K9me1 is converted in the nucleus to H3K9me3 by the Suv39h enzymes to reinforce heterochromatin. Simultaneous depletion of Prdm3 and Prdm16 abrogates H3K9me1 methylation, prevents Suv39h-dependent H3K9me3 trimethylation, and derepresses major satellite transcription. Most strikingly, DNA-FISH and electron microscopy reveal that combined impairment of Prdm3 and Prdm16 results in disintegration of heterochromatic foci and disruption of the nuclear lamina. Our data identify Prdm3 and Prdm16 as H3K9me1 methyltransferases and expose a functional framework in which anchoring to the nuclear periphery helps maintain the integrity of mammalian heterochromatin.

INTRODUCTION

Mammalian heterochromatin has important functions for genome organization, chromosome segregation, and in stabilizing gene expression programs. In mouse fibroblasts, pericentric heterochromatin clusters into distinct heterochromatic foci, which can be visualized by DAPI-staining of the underlying A/T-rich satellite repeats. In addition to this characteristic concentration into heterochromatic foci, a biochemical pathway for the Suv39h enzymes to induce H3K9me3 and binding of HP1 is a hallmark for mammalian heterochromatin (Bannister et al., 2001; Lachner et al., 2001; Rea et al., 2000). Loss of the Suv39h KMTs significantly impairs heterochromatic modification patterns and results in reduction of H3K9me3 to H3K9me1 but allows preservation of heterochromatin organization within DAPI-dense foci (Peters et al., 2003). These data indicate that other mechanisms, such as H3K9me1, initiate and precede Suv39h function at pericentric heterochromatin.

Several additional enzymes participate in heterochromatin formation (e.g., Hdac1, Eset/Setdb1, Suv4-20h, and Dnmt3a/b; for review see Fodor et al., 2010), and a substochiometric complex containing Suv39h, Eset, and G9a/Glp1 has been described (Fritsch et al., 2010). For both Suv39h and Suv4-20h deficiency, there is conversion to the monomethyl state but not to the fully unmodified state (Peters et al., 2003; Schotta et al., 2008). These data expose an important function for histone monomethylation and suggest two-step pathways for the establishment of H3K9me3 and H4K20me3 that require pre-existing H3K9me1 and H4K20me1. Monomethylating KMTs appear to be essential enzymes because their loss-of-function is embryonic lethal and defies cell viability. For example, knockout of the H4K20 monomethylase Pr-Set7 blocks development of mouse embryos prior to the eight cell stage (Oda et al., 2009). Also, loss of Eset results in early embryonic lethality starting at day E3.5 (Dodge et al., 2004). Importantly, this enzyme can convert unmodified substrates to a monomethyl state but also acts progressively toward the generation of H3K9me3 (Loyola et al., 2009; Wang et al., 2003).

H3K9me1 has been shown to be present in the free pool of histones in the cytoplasm and nucleus. This is prominent for H3K9me1 (and H3K9me2) because most of the other histone

methylation marks cannot be detected in nonnucleosomal histones (Loyola et al., 2006). We used a biochemical assay to identify enzymes that will convert an unmodified histone peptide to the H3K9me1 state and be inactive toward a H3K9me1 substrate. This analysis discovered Prdm3 and Prdm16 as H3K9me1-specific KMTs. The mammalian Prdm/PRDM family of SET domain enzymes consists of 17 members and is characterized by the combination of a PR-SET domain with a variable number of Zn-fingers (Fumasoni et al., 2007). It includes important regulators for chromatin function (e.g., PRDM2/RIZ and Prdm9/Meisetz) (Hayashi et al., 2005; Kim et al., 2003) and transcription-factor-like activities that are involved in cell fate determination (e.g., Prdm1/Blimp and Prdm14) (Ma et al., 2011; Ohinata et al., 2005; Yamaji et al., 2008). Prdm3 and Prdm16 serve important functions in hematopoietic (Aguilo et al., 2011; Goyama et al., 2008) and neuronal stem cells (Chuikov et al., 2010) and in adipose tissue differentiation (Seale et al., 2008) but have also been described as oncoproteins (Mel1 and Evi1) in translocation-induced leukemia (Mochizuki et al., 2000; Morishita, 2007; Perkins et al., 1991). Although these functions for Prdm3 and Prdm16 are well documented, no role in heterochromatin formation has been evident. This is probably because their gene function could be redundant, as has often been the case for mammalian heterochromatin components. Similar observations have been made for Suv39h1 and Suv39h2 (Peters et al., 2001), Suv4-20h1 and Suv4-20h2 (Schotta et al., 2008), Dnmt3a and Dnmt3b (Okano et al., 1999), and for transcription factors (e.g., Pax3 and Pax9) that repress RNA output from heterochromatic repeat sequences (Karslioglu et al., 2012).

Based on the biochemical definition of Prdm3 and Prdm16 as H3K9me1 KMTs, we analyzed their contribution to mammalian heterochromatin formation by simultaneously depleting Prdm3 and Prdm16 in mouse embryonic fibroblasts. Our data demonstrate that Prdm3 and Prdm16 initiate heterochromatin formation by inducing cytoplasmic H3K9me1, which is then converted in the nucleus by the Suv39h enzymes to H3K9me3. Most notably, Prdm3 and Prdm16 are also required to maintain the subnuclear organization of mammalian heterochromatin because their impaired function dissolves DAPI-dense foci and unstructures the nuclear lamina. Our work thus discovers Prdm3 and Prdm16 as H3K9me1-specific enzymes in a sequential pathway that defines heterochromatic H3K9 methyl marks. In addition, it exposes a functional framework in which the anchoring to the nuclear lamina appears as an important mechanism to protect the integrity of mammalian heterochromatin.

RESULTS

Purification of H3K9me1-Specific Methyltransferases

To develop a biochemical assay that would allow the identification of specific H3K9me1 KMTs, we first analyzed the distribution of H3K9 methylation in different cellular compartments. For this, histones were acid-extracted from cytoplasmic and nuclear fractions and subsequently probed with antibodies directed against unmodified histone H3, H3K9me1, H3K9me2, and H3K9me3. In HeLa cells all H3K9 methylation states are present in the nucleus, but in the cytoplasm only H3K9me1

and H3K9me2 are detected (Figure 1A), which is in line with previous reports (Loyola et al., 2006). Although wild-type (WT) immortalized mouse embryonic fibroblasts (iMEFs) display the same distribution as human cells, *Suv39h* double null (*Suv39h* dn) iMEFs are depleted for nuclear H3K9me3 (Figure 1A). This experiment confirmed that H3K9me1 occurs in the cytoplasm and nucleus of human and mouse cells and suggests that the responsible enzyme(s) might reside in both cellular compartments.

We next performed in vitro methyltransferase assays with cytoplasmic and nuclear extracts of HeLa cells. The radioactive methyl group of S-adenosylmethionine (SAM) is efficiently transferred onto recombinant histone H3 in both extracts (Figure 1B). However, full-length histone H3 as a substrate does not allow discrimination between different methylation sites or methylation states. Therefore, we used histone peptides spanning the H3K9 position, either unmodified or monomethylated at lysine 9. A longer H3K9 peptide (amino acid [aa] 1–20) is again methylated in both extracts independently of its H3K9 methylation status. We next tried a very short peptide containing aa 6–11 (TARKST-2b), where lysine 9 is the only lysine in this substrate. These peptides were synthesized as branched molecules and present two linear aa sequences that are covalently linked by a C-terminal cysteine (so called two-branched, or 2b, peptides) (Peters et al., 2003). Strong and comparable enzymatic activities toward the unmodified TARKST-2b, but not toward the TARK(me1)ST-2b, peptide were observed in both cytoplasmic and nuclear extracts (Figure 1B).

For the initial purification, we decided to focus on cytoplasmic fractions because we detected substantial amounts of this modification in the cytoplasm (Figure 1A) and because H3K9me1 has been described as a prominent modification of nonnucleosomal histones (Loyola et al., 2006). To identify H3K9me1-specific KMT(s), HeLa S100 extracts were subjected to a series of chromatography columns (detailed purification scheme in Figure 1C) and the H3K9me1 activity in the eluted fractions was monitored via radioactive KMT assays by using the short TARKST-2b and TARK(me1)ST-2b peptides as substrates (Figure 1E). After the last gel filtration column, odd-numbered fractions were used in KMT assays (Figure 1E), and their protein content was visualized on silver-stained SDS gels (Figure 1D). Fractions 19 through 39 displayed the activity profile of a specific H3K9 mono-KMT: active on the unmodified, but inactive on the TARK(me1)ST-2b peptide (Figure 1E). After resolution on a silver-gel, we observed two distinct banding patterns: in fractions 19–25 there was hardly any bands visible, whereas fractions 27–39 contained up to 4 prominent bands. To not exclude any enzymes, we used one representative fraction of the remaining even-numbered fractions (24 and 30) for in-solution digests and mass spectrometry (MS)-based protein identification.

Analysis of sequenced peptides identified ~500 proteins within these two fractions, including 32 proteins with a described chromatin connection (for a detailed listing see Table S1 available online). Next to DNA replication complexes, nuclear transport factors, and protein chaperones, there were also several enzymes such as acetyltransferases/deacetylases and methyltransferases/demethylases. Most notably, four
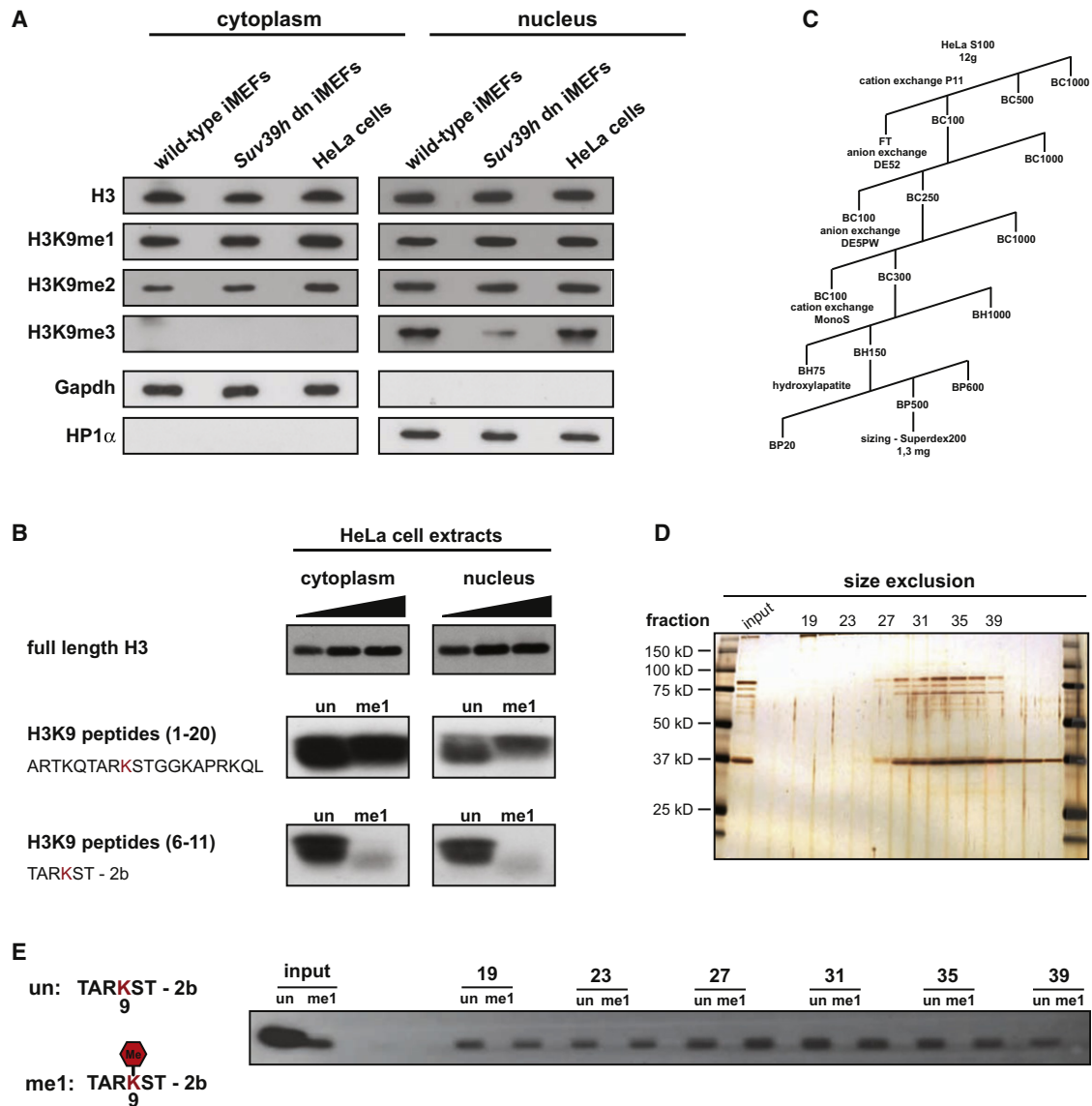
Figure 1. Purification of H3K9me1 Enzymes

(A) Western blot analysis of H3K9 methylation states in cytoplasmic and nuclear extracts of WT iMEFs, *Suv39h* dn iMEFs and HeLa cells. Acid-extracted histones were probed with modification-specific antibodies for unmodified H3, H3K9me1, H3K9me2, and H3K9me3. Antibodies against Gapdh (cytoplasmic) and HP1α (nuclear) were used as a control.

(B) H3K9me1 KMT activity in cytoplasmic and nuclear extracts of HeLa cells. Extracts were incubated with radioactive SAM and the following H3 substrates: recombinant H3; H3 (aa 1–20) peptides, unmodified and H3K9me1; H3 (aa 6–11) peptides, unmodified (TARKST-2b) or H3K9me1 (TARK(me1)ST-2b). Incorporation of the radioactive methyl group from the SAM donor is visualized by autoradiography.

(C) Purification scheme for H3K9me1 KMT activity from HeLa S100 cytoplasmic extracts.

(D) Silver-stained SDS gel of active fractions after the last gel filtration column.

(E) KMT activity assay of these fractions on H3 (6–11) peptides, either unmodified (TARKST-2b) or H3K9me1 (TARK(me1)ST-2b). Incorporation of the radioactive methyl group from the SAM donor is visualized by autoradiography. See also Figure S1 and Table S1.

(i.e., PRDM16, ESET/SETDB1, SETD5, and ASH1L) of the identified proteins contain the conspicuous SET domain, the hallmark of most KMTs (Figure 2A), and therefore represented strong candidates for H3K9me1 KMTs. In addition, we also noticed the arginine methyltransferase PRMT5 as a prominent hit among the identified peptide fragments. Because PRMT5 has been described to modify histone H3 on arginine 8 (H3R8) (Pal et al., 2004), our assay design using the short H3 peptides (aa 6–11) might also select for such an activity. Although this is indeed the case (Figure S1A), our subsequent analysis using Prmt5 knockdown in iMEFs did not indicate a role for this enzyme in heterochromatin formation (Figure S1B).

Prdm3 and Prdm16 Specifically Convert H3K9 to H3K9me1 In Vitro

For the subsequent study, we focused our analysis on the mouse orthologs of the four identified SET domain proteins, PRDM16, ESET, ASH1L, and SETD5. Although Eset has been previously reported to mediate H3K9me1 and H3K9me3 (Loyola et al., 2009; Wang et al., 2003), mammalian Ash1L had only been described to target H3K4 and H3K36 (An et al., 2011; Gregory et al., 2007). Setd5 and Prdm16 had not been shown to display KMT activity. To examine the activity and specificity of these potential H3K9me1 KMTs, bacterially or baculovirus expressed proteins were incubated with recombinant H3 and cold SAM, and the induced methylation status was probed with modification-specific antibodies against H3K9 and H3K27 methylation. Due to its close homology with Prdm16 (domain structure in Figure 2A, 54% identity in the amino acid sequence), we also included Prdm3 in this analysis. All examined proteins display specificity toward the H3K9 position and do not methylate H3K27 (Figure 2B), even though these two lysines reside in a very similar sequence context (ARKS motif). Prdm3, Prdm16, Setd5, and Ash1L act as H3K9me1 mono-KMTs in this assay because they induce H3K9me1 but do not generate H3K9me3. In line with previous reports (Loyola et al., 2009; Wang et al., 2003), histones that were incubated with baculovirus expressed Eset are recognized by H3K9me1 and H3K9me3 antibodies, showing that this KMT is not an exclusive mono-KMT (Figure 2B). Because Ash1L exhibited only very weak activity toward H3K9me1 and had been described to be involved in active transcription (Gregory et al., 2007), and Setd5 knockdown in iMEFs did not affect heterochromatin integrity (data not shown), we decided to focus our further analysis on Prdm3 and Prdm16 as H3K9me1 KMTs.

We next sought to validate the specificity of Prdm3 and Prdm16 toward H3K9me1 by an antibody-independent method. For this, the reaction products of short linear H3 (aa 6–11) peptides that had been incubated with recombinant Prdm3 or Prdm16 were analyzed by MS. When an unmodified peptide was used as substrate, Prdm3 and Prdm16 exclusively generate monomethylation, with conversion rates ranging from 15.6% for Prdm16 to 20.9% for Prdm3 (Figure 2C). The observed shift in the corresponding mass spectra confirms the addition of only one methyl-group (Figure 2C). The subsequent MS/MS analysis proved that it is lysine 9 that is methylated (see Table S2). Importantly, the H3K9me1 peptide cannot be used as a substrate by the Prdm3 or Prdm16 enzymes (Figure 2C). Taken together, these data demonstrate that Prdm3 and Prdm16 act as H3K9me1-specific KMTs in vitro.

Simultaneous Depletion of Prdm3 and Prdm16 Abrogates Pericentric H3K9me3 and H3K9me1

To address the role of Prdm 3 and Prdm16 for H3K9me1 in vivo, we generated lentiviral shRNA constructs to knock down their expression in immortalized mouse embryonic fibroblasts (iMEFs). As a control, we also included the previously described Eset/Setdb1 in this analysis. Multiple sequences for each mRNA sequence were screened, and the most effective shRNA was chosen for virus production (Figure S2). Interestingly, one of the shRNAs designed for Prdm16 also targeted Prdm3, thereby

allowing for an effective double knockdown using a single shRNA construct (sh16/3; Figures S2B and S2C). We first performed knockdowns in WT iMEFs, which display an accumulation of H3K9me3 at DAPI-dense foci and a broad nuclear staining of H3K9me1. Time points were taken at day 3, 6, and 12 after infection and indirect immunofluorescence (IF) with H3K9 methyl antibodies was carried out. Single knockdown of Eset, Prdm3, or Prdm16 did not result in a detectable alteration as compared to control cells (scrambled shRNA) (Figure 3A). By contrast, double knockdown of Prdm3 and Prdm16 abolished the pericentric localization of H3K9me3 in more than 50% of the cells (Figure 3A).

We next infected Suv39h dn iMEFs with the lentiviral shRNA constructs. In Suv39h dn cells, H3K9me3 is lost from DAPI-dense foci, which instead accumulate H3K9me1 (Peters et al., 2003) (Figure 3B). Therefore, these cells provide an ideal resource to directly examine dependence of pericentric H3K9me1 on Prdm3, Prdm16, or Eset enzymes. IF analysis with H3K9me1-specific antibodies revealed that simultaneous depletion of Prdm3 and Prdm16 significantly disperses pericentric H3K9me1 (ranging from 70% of cells at day 3 to 94% of cells at day 12), whereas single knockdowns of Prdm3 and Prdm16 have no effect (Figure 3B). Depletion of Eset in Suv39h dn iMEFs also interferes with pericentric H3K9me1 accumulation because only 50%–33% of the cells maintain a focal enrichment for H3K9me1 (Figure 3B). This result indicates that Eset contributes to H3K9me1 at pericentric heterochromatin in Suv39h dn cells. Importantly, our data reveal that Prdm3 and Prdm16 are redundant H3K9me1 KMTs and specify a sequential pathway, in which Prdm3/Prdm16-dependent H3K9me1 is important for the subsequent conversion to H3K9me3 at pericentric heterochromatin by the Suv39h enzymes.

In addition to the H3K9me1 and H3K9me3 marks, we also examined other histone modifications (H3K27me1 and H4K20me3), DNA methylation (5-methylcytosine, 5-meC) and chromatin-associated factors (e.g., HP1α) of pericentric heterochromatin. For all these marks and factors, there is significant dispersion from pericentric heterochromatin in Prdm3/Prdm16-depleted iMEFs (Figure S3A). Further, and as already described for the absence of the Suv39h enzymes (Martens et al., 2005), there is pronounced loss of silencing of major satellite (major sat) transcription in Prdm3/Prdm16-deficient WT and Suv39h dn iMEFs (Figure S3B). Enhanced derepression of major sat transcription is also observed upon depletion of Eset in Suv39h dn iMEFs, but not in WT iMEFs (Figure S3B).

With all these defects in heterochromatin definition, it is not surprising that Prdm3/Prdm16-depleted iMEFs show progressive impairment of cell viability both in WT and, even more evident, in Suv39h dn cells. This is not a consequence of cell death/apoptosis because there are less than 1% of WT or Suv39h dn iMEFs that are positive for cleaved caspase 3 (data not shown). Examination of cell-cycle progression by 5′-Bromo-2′-Deoxyuridine (BrdU) incorporation indicates that replication has largely stopped by day 6 after infection (Figure S4A), with a significant number of WT iMEFs staining positive for the senescence marker β-Galactosidase (Figure S4B). Consistent with similar observations (Reimann et al., 2010), Suv39h dn iMEFs lack cellular senescence and do not display
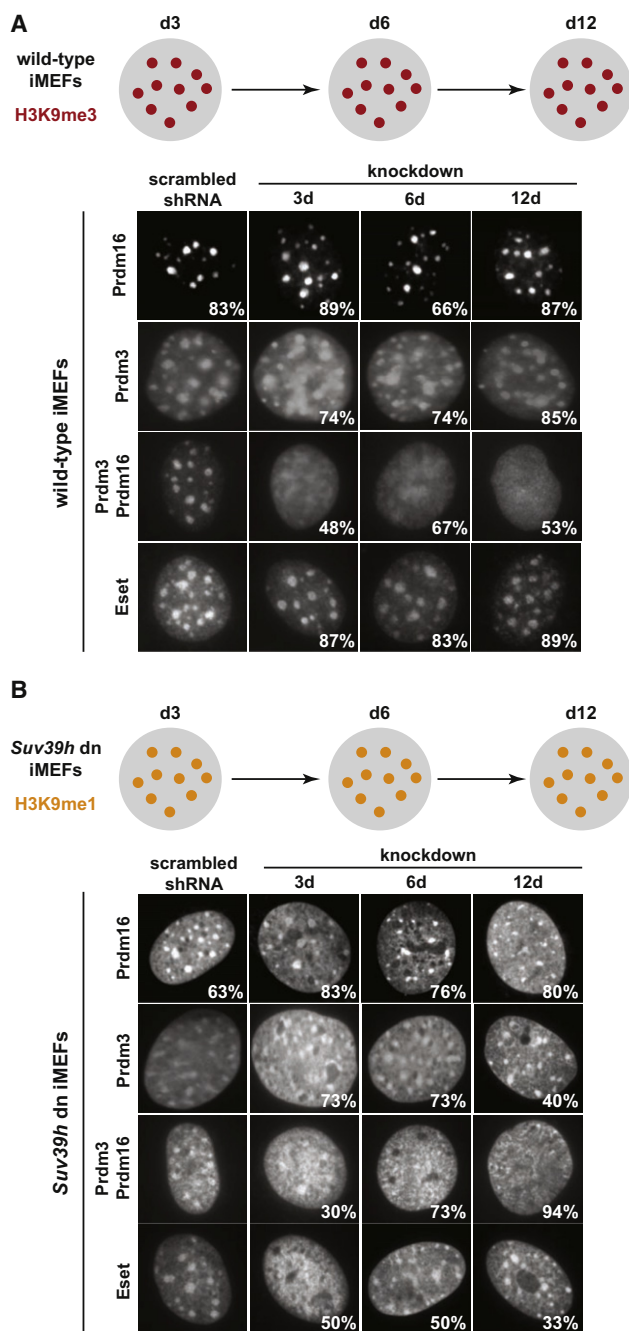
Figure 2. Prdm3 and Prdm16 Convert H3K9 to H3K9me1 In Vitro

(A) Domain structure of candidate H3K9me1 KMTs identified by MS. The PR-SET and SET domain are highlighted in light red, pre- and post-SET domain in dark red, Zn-fingers (Zn-F) in light gray, Tudor domain and PhD fingers in dark gray, Bromo domain and methyl-binding domain (MBD) in green. Blue arrows demarcate the protein portions that were used as recombinant enzymes in KMT assays described below.

(B) KMT activity assay with candidate H3K9me1 methyltransferases. Recombinant enzymes were incubated with cold SAM and full-length histone H3. Induced methylation states are visualized by western blot analysis with modification-specific antibodies directed against H3K9me1, H3K9me2, H3K9m3 and H3K27me1, H3K27me2, and H3K27me3.

(C) MS analysis of Prdm3 and Prdm16 activity. Recombinant enzymes were incubated with cold SAM and linear H3 (aa 6–11) peptides, unmodified (TARKST), or H3K9me1 (TARK(me1)ST). Reaction products were purified by nanoHPLC and then analyzed by MS. HPLC peaks are shown for both substrates. For better illustration, HPLC peaks corresponding to unmodified (red) and H3K9me1 (blue) peptides were separated, as indicated by the color-coded x axes below. For the unmodified peptide the corresponding mass spectra are included, demonstrating a shift in mass by 14 Da. See also Figure S1 and Tables S1 and S2.

Figure 3. Simultaneous Depletion of Prdm3 and Prdm16 Abrogates Pericentric H3K9me3 and H3K9me1

(A) Immunofluorescence analysis for H3K9me3 in WT iMEFs upon shRNA mediated knockdown of Eset, Prdm3, Prdm16, and double knockdown of Prdm3/Prdm16. Representative images at days 3, 6, and 12 after shRNA transduction are shown. Percentages indicate cells that display the depicted phenotype.

(B) Immunofluorescence analysis for H3K9me1 in *Suv39h* dn iMEFs upon shRNA mediated knockdown of Eset, Prdm3, Prdm16, and double knockdown of Prdm3/Prdm16. Representative images at days 3, 6, and 12 after shRNA transduction are shown. Percentages indicate cells that display the depicted phenotype.

See also Figures S2, S3, and S4.

β-Galactosidase signals. However, Prdm3/Prdm16 depletion in *Suv39h* dn iMEFs results in acute reduction of the overall cell numbers, indicating that the combined absence of H3K9me1 (Prdm3/Prdm16) and H3K9me3 (Suv39h1 and Suv39h2) methylation systems defies cellular viability.

Prdm3 and Prdm16 Primarily Regulate H3K9me1 in the Cytoplasm

Our purification of the PRMD16 KMT from cytoplasmic extracts strongly suggests that this (and the closely related PRDM3) enzyme mediates H3K9me1 in a nonnucleosomal context. However, the observed defects for H3K9me1 and H3K9me3 localization at pericentric heterochromatin upon Prdm3/Prdm16-depletion occur in the nucleus. Isolation of acid-extracted histones from the cytoplasm and nucleus indicates specific reduction of cytoplasmic, but not nuclear, H3K9me1 levels in Prdm3/Prdm16-deficient iMEFs (Figure 4A). We did not detect changes in the abundance of cytoplasmic H3K9me2, nor of bulk nuclear H3K9me1, H3K9me2, and H3K9me3. Although Eset has also been implicated as a H3K9me1 KMT (Loyola et al., 2009), our Eset knockdown conditions did not result in any apparent alterations of either cytoplasmic or nuclear H3K9 methylation levels (Figure 4A). To address modulation of H3K9me1 and H3K9me3 at the major sat repeat sequences, we next performed directed chromatin immunoprecipitation (ChIP) in WT and *Suv39h* dn iMEFs that had been depleted for Prdm3/Prdm16 or for Eset. Although there is a similar, yet modest, decline for pericentric H3K9me1 signals in *Suv39h* dn cells, major sat H3K9me3 levels in WT iMEFs are considerably more reduced upon Prdm3/Prdm16 knockdown as compared to Eset depletion (Figure 4B).

These data might imply that the Prdm3 and Prdm16 enzymes could also directly reside at pericentric heterochromatin. Because robust antibodies for ChIP analysis of endogenous Prdm3 and Prdm16 are lacking (and our attempts to generate custom-made antibodies failed), we generated iMEF cell lines that stably express either 3xFLAG-HA-tagged Prdm3 (Prdm3-F/H) or Prdm16 (Prdm16-F/H) (Figures S5A and S5B). We also established a third cell line that gives rise to a deletion mutant lacking the PR-SET domain of Prdm16 (Prdm16ΔPR-F/H). Although this mutant is significantly less active, immunoprecipitated Prdm16ΔPR-F/H is still able to methylate an unmodified H3 peptide (Figure S5C), probably because of interaction with endogenous Prdm16 and/or Prdm3. We therefore did not include this mutant in the subsequent ChIP experiments.

To analyze chromatin association of the ectopic Prdm3-F/H and Prdm16-F/H enzymes (using a combination of α-FLAG and α-HA antibodies), we performed directed ChIP for the major sat repeats and, as controls, also for two described Prdm3 target genes (*Gadd45g*, *Dcn*) and at one nontarget gene (*Plagl1*) (Yatsula et al., 2005). Although both Prdm3-F/H and Prdm16-F/H accumulate at the Gadd45g and Dcn promoters, they are not enriched at the major sat repeats (Figure 4C). Moreover, H3K9me1 and H3K9me3 signals at the *Gadd45g* and *Dcn* target regions are unaltered in Prdm3-F/H or Prdm16-F/H iMEFs as compared to WT controls, and chromatin association of Prdm3-F/H and Prdm16-F/H does not appear to correlate with increased H3K9me1 (or H3K9me3) levels (Figure 4C). This is
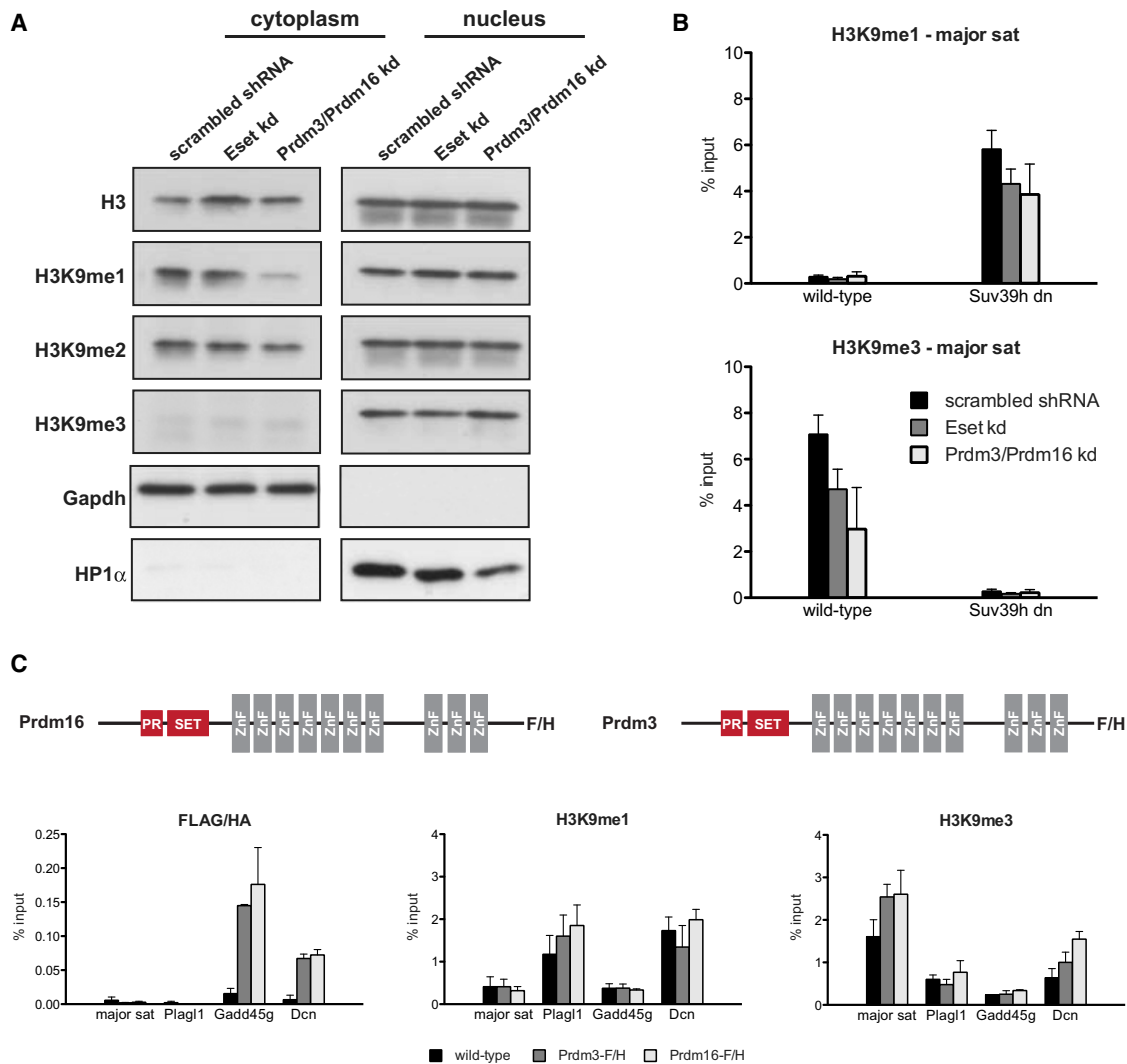
Figure 4. Prdm3 and Prdm16 Primarily Regulate H3K9me1 in the Cytoplasm

(A) Western blot analysis of H3K9 methylation states in cytoplasmic and nuclear extracts of WT and *Suv39h* dn iMEFs upon Eset and Prdm3/Prdm16 double knockdown. Acid-extracted histones were probed with modification-specific antibodies for unmodified H3, H3K9me1, H3K9me2, and H3K9me3. Antibodies against Gapdh (cytoplasmic) and HP1α (nuclear) were used as fractionation controls.

(B) Histogram for ChIP analysis of major sat repeats in WT and *Suv39h* dn iMEFs upon Eset and Prdm3/Prdm16 double knockdown with antibodies directed against H3K9me1 and H3K9me3. Error bars represent SD.

(C) Histogram for ChIP analysis of 3xFLAG-HA-tagged Prdm3 and Prdm16 in WT iMEFs. Occupancy of the ectopic proteins was analyzed at major sat repeats, two described Prdm3 targets (*Gadd45g*, *Dcn*) and one Prdm3 nontarget (*Plagl1*). In addition, methylation levels at these regions were probed with H3K9me1 and H3K9me3 antibodies. Error bars represent SD.

See also Figure S5.

a surprising result, suggesting that Prdm3 and Prdm16 either cannot modify nucleosomes or that the nucleosomal H3K9 position is not an available substrate. The functions of Prdm3 and Prdm16 at the Gadd45g and Dcn (and other) target promoters will probably involve activities that are distinct from methylating free histone H3. Taken together, these collective data exclude a direct localization of the Prdm3 and Prdm16 at pericentric heterochromatin, but are consistent with an indirect mechanism that involves a deposition-based model for Prdm3/Prdm16-dependent H3K9me1 of free histone H3 in the cyto-

plasm and its subsequent nuclear incorporation into pericentric heterochromatin.

Impaired Prdm3/Prdm16 Function Disintegrates Heterochromatic Foci and Breaks Heterochromatin Organization

We noticed from the above IF analyses (Figure 3 and Figure S3A) that Prdm3/Prdm16 knockdown reproducibly induces diffuse DAPI staining and, in extreme cases, even dissolves DAPI-dense foci that are formed by the clustering of the A/T-rich major sat
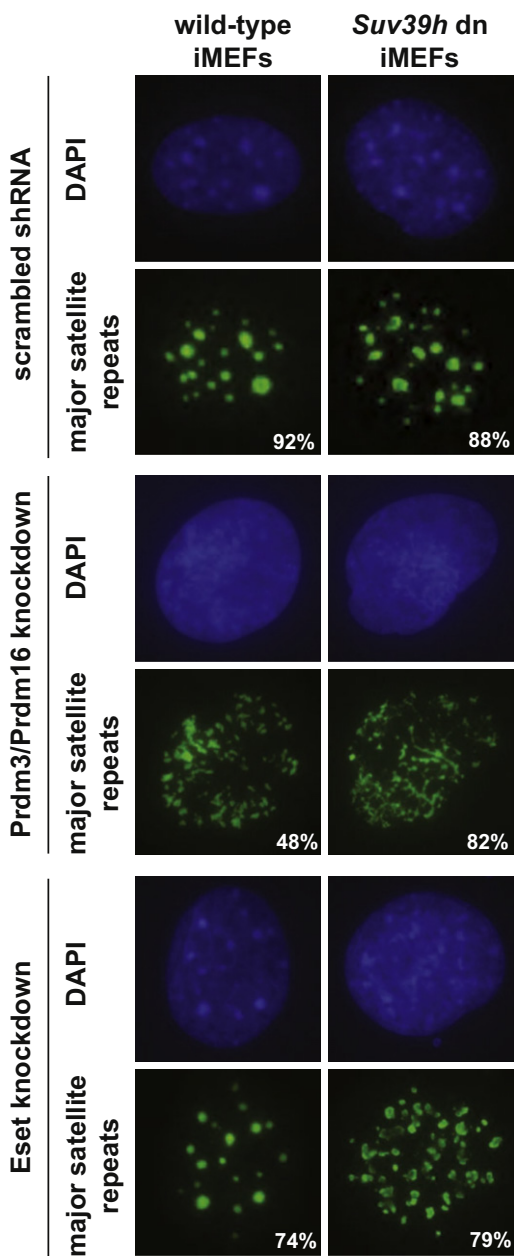
Figure 5. Impaired Prdm3/Prdm16 Function Disintegrates Heterochromatic Foci

DNA-FISH for major sat repeats in WT and *Suv39h* dn iMEFs upon Eset and Prdm3/Prdm16 double knockdown. Representative images at day 3 after shRNA transduction are shown. Percentages indicate cells that display the depicted phenotype. See also Figures S6 and S7.

repeats. To directly analyze the organization of DAPI-dense heterochromatic foci, we performed DNA-FISH with probes that are specific for the major sat repeats. In control cells treated with scrambled shRNA, the DNA-FISH signal for major sat repeats perfectly overlaps with DAPI-dense focal staining, both in WT and *Suv39h* dn iMEFs (Figure 5, top). This finding illustrates that loss of pericentric H3K9me3 (and H4K20me3 and HP1α) in

Suv39h dn cells is not sufficient to alter heterochromatic DNA organization. Similarly, knockdown of Eset in WT cells did not significantly affect the focal arrangement of major sat repeats, whereas the DNA-FISH signals appear more decondensed in *Suv39h* dn iMEFs (Figure 5, bottom). This result suggests a possible compensation by the Eset enzyme in protecting the heterochromatic structure, if it still contains H3K9me1. By contrast, simultaneous depletion of Prdm3 and Prdm16 leads to a dramatic impairment of major sat organization: the focal accumulation is entirely abolished and the remaining DNA-FISH signals resemble a network of disentangled chromatin fibers (Figure 5, middle). This collapse is more pronounced in *Suv39h* dn (observed in 82% of cells) as compared to WT iMEFs (observed in 48% of cells). The massive dissolution of heterochromatic foci in Prdm3/Prdm16 iMEFs represents the most dramatic breakdown for heterochromatin organization and significantly exceeds heterochromatic defects, as they are described for *Suv39h* dn cells (Peters et al., 2003; Peters et al., 2001), *Suv4-20h* dn cells (Schotta et al., 2008), Eset knockdown cells (see Figure 5), *Dnmt3a/Dnmt3b* dn cells (Lehnertz et al., 2003; Okano et al., 1999), and *Pax3/Pax9* deficient cells (Karslioglu et al., 2012).

To exclude any off-target effects and to validate this central result, we depleted Prdm3 and Prdm16 by the combined transduction of shRNAs (shPrdm3 + shPrdm16, each with different sequence selectivity as compared to the double-knockdown sh16/3 lentivirus; Figures S2B and S2C) in WT and *Suv39h* dn iMEFs, which recapitulates disintegration of heterochromatic foci (Figure S6). In addition, we also derived *Prdm3* null (Goyama et al., 2008) and Prdm16-deficient iMEFs from mutant mice. IF for H3K9me3 and DNA-FISH indicates that 35% of *Prdm3* null iMEFs display dissolved heterochromatic clusters (Figure S7), whereas Prdm16-deficient cells appear normal for heterochromatin organization but show aberrant staining for Lamin A/C in the nuclear periphery (see below).

Depletion of Prdm3/Prdm16 Also Unstructures the Nuclear Lamina

Considering the severe defects in cell viability (see above) upon simultaneous depletion of Prdm3 and Prdm16, we wanted to exclude that the disintegration of heterochromatin is due to an overall breakdown of nuclear integrity. We therefore analyzed other prominent nuclear structures, such as nucleoli and the nuclear lamina. Nucleoli are a particularly good control because they display a distinct subnuclear localization, contain repeated DNA sequences (the rRNA gene clusters), and accumulate condensed chromatin (McStay and Grummt, 2008; Németh and Längst, 2011). IF for the nucleolar marker Fibrillarin shows that the nucleolar structure is not altered upon simultaneous depletion of Prdm3/Prdm16 in WT iMEFs (Figure 6A). Although WT cells contain around four to five large nucleoli, *Suv39h* dn iMEFs have, on average, 12 smaller Fibrillarin-positive foci (Figure 6A). This is consistent with previous analyses in *Drosophila* that implicate SU(VAR)3-9 in determining nucleoli numbers (Peng and Karpen, 2007). Despite this difference, Prdm3/Prdm16 double knockdown did not further affect Fibrillarin localization or nucleolar definition in WT or *Suv39h* dn iMEFs.
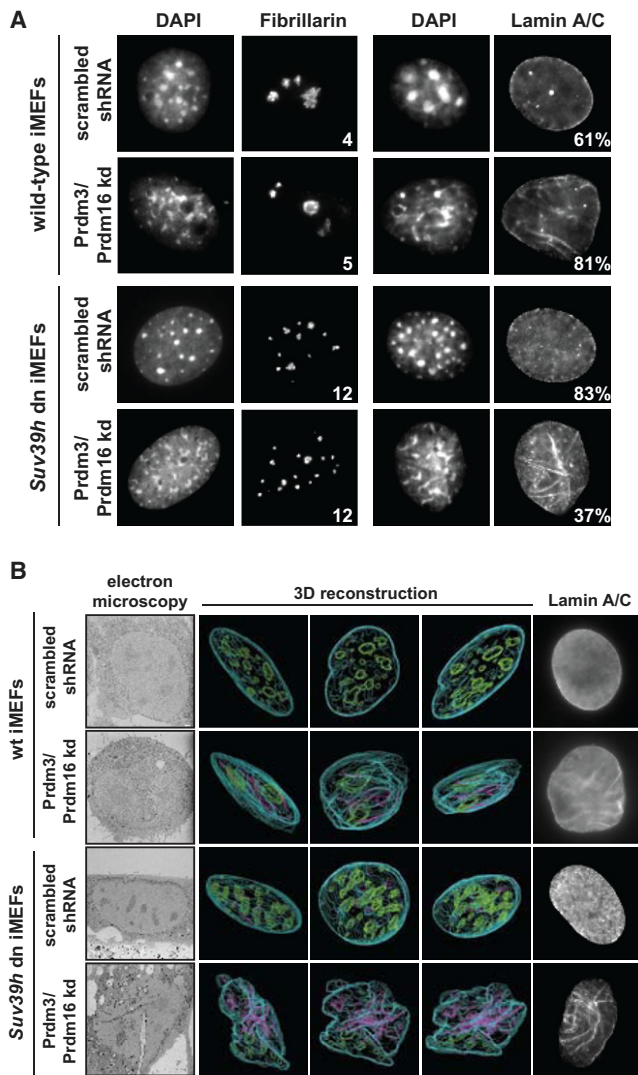
Figure 6. Depletion of Prdm3/Prdm16 Unstructures the Nuclear Lamina

(A) Immunofluorescence analysis for marker proteins of nucleoli (Fibrillarin) and the nuclear lamina (Lamin A/C) in WT and *Suv39h* dn iMEFs upon double knockdown of Prdm3/Prdm16. Representative images at day 3 after shRNA transduction are shown. Numbers in the left panels represent number of nucleoli and percentages in the right panels indicate cells that display the depicted phenotype.

(B) EM images and 3D reconstructions of one representative cell for either WT and *Suv39h* dn iMEFs upon control and Prdm3/Prdm16 double knockdown. Three serial sections are displayed for each cell. Heterochromatic regions are highlighted in green, the nuclear lamina is depicted in blue and invaginations of the nuclear membrane are shown in purple. In addition, Lamin A/C stainings are included.

We next examined the nuclear lamina because this structure has been described to interact with mammalian heterochromatin (Kind and van Steensel, 2010; Towbin et al., 2009). HP1 proteins have been shown to directly bind to the Lamin B receptor, which could provide a mechanism to anchor pericentric heterochromatin at the nuclear periphery (Ye et al., 1997). To analyze the integrity of the nuclear lamina upon Prdm3/Prdm16 double

knockdown, we stained WT and *Suv39h* dn iMEFs for Lamin A/C at day 3 after shRNA infection. In control (scrambled shRNA) iMEFs, Lamin A/C localizes to the nuclear envelope with a ring-like staining in WT and a more diffuse, yet rim-associated distribution, in *Suv39h* dn cells (Figure 6A). By contrast, depletion of Prdm3/Prdm16 results in an aberrant pattern of the Lamin A/C signals in WT and *Suv39h* dn cells. Although there are more affected cells in WT iMEFs (81%) as compared to *Suv39h* dn iMEFs (37%), Prdm3/Prdm16-depletion in *Suv39h* dn iMEFs results in a more pronounced unstructuring of the nuclear lamina. The laminar proteins are no longer aligned along the nuclear envelope but fuse into disordered patches at the nuclear rim and within the nucleus (Figure 6A).

To analyze the dissolved heterochromatin and perturbed nuclear lamina at higher resolution, we conducted serial block-face scanning electron miscrocopy (SBFSEM) (Denk and Horstmann, 2004) of control and Prdm3/Prdm16 knockdown iMEFs (see Experimental Procedures). We then used the entire stack of SBFSEM images to reconstruct the 3D architecture of selected nuclei (Figure 6B). For these 3D reconstructions we focused on heterochromatic foci (shown in green) and the nuclear lamina (depicted in blue). In each image, the outline/contour of the nuclear lamina and of the heterochromatic foci was manually demarcated and these highlighted sections were then processed for a 3D reconstruction using Neurolucida software (see Experimental Procedures). This high-resolution EM analysis illustrates the significant disintegration of heterochromatin and concurrent defects in nuclear lamina organization in Prdm3/Prdm16 knockdown cells (Figure 6B). In addition, the invaginations of the nuclear envelope, (highlighted in purple) are particularly evident and appear more pronounced upon depletion of Prdm3 and Prdm16 in *Suv39h* dn iMEFs.

DISCUSSION

The Prdm3 and Prdm16 H3K9me1 Methyltransferases Are Multifunctional Factors

Our study identifies Prdm3 and Prdm16 as H3K9me1 KMTs that safeguard heterochromatin structure and organization. Both enzymes are members of the Prdm protein family, which is characterized by the combination of a PR-SET domain with a variable number of Zn-fingers (Fumasoni et al., 2007) (see Figure 2A). The PR-SET module is related to the classical SET domain and contains all critical residues required for KMT activity (Huang, 2002). Thus, this unique combination of a catalytic domain with DNA-recognition motifs predicts (at least) a dual role for Prdm proteins: as histone-modifying enzymes (mediated via the PR-SET domain) and as bona-fide transcription factors (via the Zn-fingers). Moreover, our data show that Prdm3 and Prdm16 work as cytoplasmic enzymes to direct H3K9me1 on free histone H3 (Figures 2 and 4), are present in the nucleus at described target gene loci (but not at pericentric heterochromatin) (Figure 4), and are essential to maintain heterochromatin clustering (Figure 5) and the structure of the nuclear lamina (Figure 6). It is unlikely that all of these functions are solely mediated by their H3K9me1 activity. This is particularly evident because chromatin association of Prdm3 and Prdm16 does not directly correlate with increased H3K9me1 (and H3K9me3) at their target genes
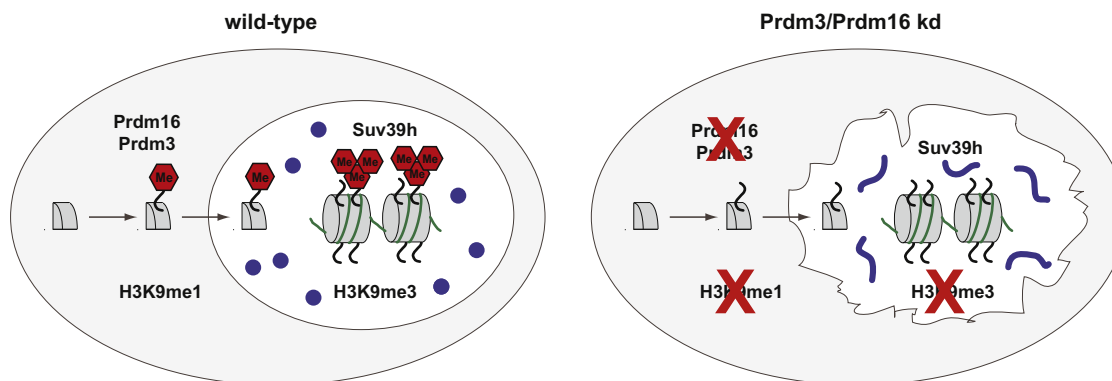
Figure 7. Deposition-Based Model for the Initiation and Maintenance of Mammalian Heterochromatin

In WT iMEFs, Prdm3 and Prdm16 direct H3K9me1 of cytoplasmic histone H3, which is then transported to the nucleus and incorporated into nucleosomes where it is converted by the Suv39h enzymes to H3K9me3 at heterochromatic foci (blue dots) that correspond to clusters of major satellite repeats. Upon Prdm3/Prmd16-depletion, cytoplasmic H3K9me1 is diminished, leading to insufficient generation of pericentric H3K9me3 by the Suv39h enzymes. In addition to the reduction of H3K9me1 (and H3K9me3) at pericentric heterochromatin, impaired Prdm3/Prdm16 function also results in the collapse of the major satellite repeat clusters (blue fibers) and breaks a proposed anchor in the nuclear lamina, which becomes unstructured (disorganized black outline). This model predicts the Prdm3 and Prdm16 KMTs as multi-functional enzymes with substrates that are not restricted to histone H3. See text for detailed explanation.

(Figure 4) and because Prdm3/Prdm16-dependent defects in the nuclear lamina appear to require other modes in addition to perturbed H3K9me1 localization (see below). Thus, as is the case for many KMTs (Huang and Berger, 2008; Lan and Shi, 2009), the spectrum of possible substrates for Prdm3 and Prdm16 will, almost certainly, not be restricted to histone H3.

Whereas Prdm proteins are well conserved among vertebrates, there are significantly less Prdm family members in invertebrates (Fumasoni et al., 2007). For example, the *Drosophila* genome contains only three and the *Caenorhabditis elegans* genome only two annotated *Prdm* genes. Notably, there are no proteins that combine a SET domain with Zn-fingers in unicellular organisms such as *Saccharomyces cerevisiae* and *Schizosaccharomyces pombe* (Fumasoni et al., 2007). To address an evolutionarily conserved function for Prdm proteins in heterochromatin maintenance, *hamlet*, the closest ortholog to *Prdm3* and *Prdm16* genes in *Drosophila*, is currently examined in PEV models to reveal a predicted Su(var) phenotype (collaboration with G. Reuter, Martin Luther University Halle-Wittenberg, Germany). However, there is no clear ortholog for Prdm3/Prmd16 in *C. elegans*, where H3K9me1 and H3K9me2 appear to be mediated by the Eset/Setdb1-related enzyme MET-2 (Towbin et al., 2012, this issue of *Cell*).

A Deposition-Based Pathway for H3K9me1 at Mammalian Heterochromatin

Our analysis of the redundant H3K9me1 KMTs Prdm3 and Prdm16 suggests a deposition-based pathway for the accumulation of H3K9me1 (and H3K9me3) at mammalian heterochromatin (see model, Figure 7): the Prdm3 and Prdm16 enzymes catalyze H3K9me1 on free histone H3 in the cytoplasm, which is then transported into the nucleus, incorporated at pericentric heterochromatin and converted to H3K9me3 by the chromatin-associated Suv39h enzymes. This pathway is supported by the reduction of cytoplasmic H3K9me1 levels in Prdm3/Prdm16-depleted cells (Figure 4) and the dispersion (Figure 3) and

decreased occurrence (Figure 4B) of H3K9me1 and H3K9me3 signals at pericentric heterochromatin. A deposition-based mechanism is further indicated by the absence of ectopic Prdm3 and Prdm16 at major sat sequences (Figure 4C). For H3K9me3, the sequence of step-wise methylation seems to be conserved in *C. elegans*, where H3K9me1/H3K9me2 by MET-2 is a prerequisite for the subsequent trimethylation by SET-25, a Suv39h-like enzyme (Towbin et al., 2012, this issue of *Cell*).

Previous studies have involved other H3K9-specific enzymatic complexes at pericentric heterochromatin, such as the replication-coupled ESET/HP1α/CAF1 complex (Loyola et al., 2009) or a substochiometric G9A/GLP1/ESET/SUV39H1 complex (Fritsch et al., 2010). Eset/Setdb1 was also identified in our biochemical purification and our knockdown analysis for Eset indicates a functional connection with the Suv39h enzymes because we observe a significant upregulation of major sat transcription (Figure S3B) and partial decondensation of heterochromatic foci in *Suv39h* dn iMEFs (Figure 5). The mechanistic details of this interaction require further analysis, but it is possible that the Eset/HP1α/Caf1 complex, which mainly processes H3K9me1 (Loyola et al., 2009), could also facilitate incorporation of Prdm3/Prdm16-mediated H3K9me1 during chromatin replication. Intriguingly, the majority of peptide fragments that were co-purified with the cytoplasmic H3K9me1 activity (Figure 1D) reveal the presence of components of the replication machinery and of protein chaperones (see Table S1).

In addition to the crucial function of H3K9me1, we have previously described another monomethylation state, H3K27me1, to be enriched at pericentric heterochromatin (Peters et al., 2003). This modification is independent of the Suv39h-HP1 system because it accumulates at DAPI-dense foci in both WT and *Suv39h* dn iMEFs (Figure S3A). The responsible H3K27me1 KMT has not yet been identified, although a recent report has shown a modest reduction for H3K27me1 levels in *G9a*-null ES cells (Wu et al., 2011). It would not be inconsistent with our data for Prdm3/Prdm16 in directing H3K9me1 that such an

activity could be promoted by another Prdm enzyme. This is an intriguing possibility because we observe that truncated versions of Prdm16 that lack several Zn-fingers change its target specificity and are also capable of catalyzing H3K27me1 instead of H3K9me1 (data not shown). This finding suggests that the Zn-fingers of Prdm16 may contribute to an allosteric regulation of enzyme activity. The accumulation of H3K27me1 at heterochromatin is conserved in *Arabidopsis* and the loss of the H3K27me1-specific enzymes ATXR5 and ATXR6 results in partial decondensation of chromocenters (Jacob et al., 2009).

Prdm3/Prdm16 and the Nuclear Lamina

Simultaneous depletion of Prdm3 and Prdm16 causes the most severe dissolution of heterochromatin integrity (Figures 5 and 6B). Strikingly, this breakdown of heterochromatic foci correlates with concurrent defects in the structuring of the nuclear lamina (see model in Figure 7). In WT cells, heterochromatic anchoring could be provided by H3K9me3, HP1α or Suv39h, all of which concentrate at DAPI-dense foci. However, loss of Suv39h enzymes alone does not impair the structure of heterochromatin or the nuclear lamina (Figure 5, top, and Figure 6B). Because pericentric H3K9me3 is reduced to H3K9me1 in *Suv39h* dn cells, it is unlikely that H3K9me3 constitutes the sole heterochromatin anchor. Despite its weak affinity toward H3K9me1 (Fischle et al., 2003), HP1α might still contribute to attachment of heterochromatin to the nuclear lamina, particularly because it has been shown to bind the Lamin B receptor (Ye et al., 1997). Our data on the absence of pericentric localization of Prdm3 and Prdm16 (Figure 4C) largely exclude these enzymes or a specific Prdm3/Prdm16-containing protein complex for a direct interaction with a component of the nuclear lamina. Moreover, the functional studies on heterochromatin anchoring in mammalian cells (this work) or in *C. elegans* (Towbin et al., 2012, this issue of *Cell*) have identified different KMTs (Prdm3/Prdm16 versus MET-2/SET-25) that share similar activities (e.g., H3K9me1 methylation) but otherwise lack a comparable domain composition of the respective enzymes. We therefore propose that it is the intrinsic lysine monomethylation activity of Prdm3/Prdm16 toward H3K9 *and* a currently unknown chromatin factor or a nuclear lamina component that might be required for the structural integrity of mammalian heterochromatin. Such a nonhistone substrate would be predicted to contain the –ARKS– or a closely related target motif. Conspicuously, interrogation of the amino acid sequences of described laminar-associated components revealed the Lamin B receptor (QRKS motif) and Lamin B2 (ARKS motif) as potential substrates to be methylated by Prdm3/Prdm16. For future studies, it will be critical to dissect whether the nuclear lamina defect is a consequence of heterochromatin breakdown or caused by the impaired function of a laminar component that needs to be methylated by Prdm3 and Prdm16. Notably, interference of H3K9 methylation by the HDAC-inhibitor trichostatin A (TSA) (Taddei et al., 2001) results in dispersion of pericentric H3K9me1 and H3K9me3 localization and also partly dissolves the focal organization of major sat repeat clusters but does not unstructure the nuclear lamina (data not shown). Although the underlying molecular pathways connecting H3K9me1 deposition and heterochromatin anchoring remain to be further defined,

our discovery of the Prdm3/Prdm16 KMTs exposes these enzymes and the H3K9me1 mark as important components to initiate and secure the structural integrity of mammalian heterochromatin.

EXPERIMENTAL PROCEDURES

Fractionation of Cells and Acid Extraction of Histones

Cytoplasmic and nuclear extracts of HeLa cells and mouse fibroblasts were prepared according to standard protocols (Dignam et al., 1983). Fractionation efficiency was controlled by western blotting for Gapdh and HP1α. Histones were acid-extracted and cytoplasmic histones were further concentrated by using 10k Amicon Ultra centrifugal devices (Millipore).

Histone Methyltransferase Assays

Radioactive KMT assays were conducted as described (Nishioka et al., 2002; Schotta et al., 2004). In a typical reaction, 1 μg of full-length recombinant histone H3 (New England Biolabs) or 800 μM of histone peptides were incubated with 1 μCi of *s*-Adenosyl-L-(methyl-^{3}H)methionine (Perkin Elmer). As source of enzymatic activity, we used 2 to 5 μl cytoplasmic and nuclear extracts or immunoprecipitated enzymes (PRMT5-F, Prdm3-F/H, Prdm16-F/H, and Prdm16ΔPR-F/H). A detailed protocol for immunoprecipitation of ectopic proteins is provided in the Extended Experimental Procedures. For nonradioactive KMT assays, 0.2–1 μg of purified enzyme and 20 μM of *s*-Adenosyl-L-methionine (New England Biolabs) were used in a reaction mixture as described above. The reaction products were examined by western blotting with modification-specific antibodies for H3K9 and H3K27. Antibodies are listed in Table S3.

Biochemical Purification of H3K9me1 KMTs

HeLa S100 cytoplasmic fractions were prepared as previously described (LeRoy et al., 1998). Twelve grams of cytoplasmic protein extract was loaded on a series of chromatography columns and the H3K9me1 activity during the purification was monitored via radioactive KMT assays on H3 peptides, either unmodified (TARKST-2b) or monomethylated (TARK(me1)ST-2b). After the last sizing column, active fractions were loaded on a 10% polyacrylamide gel, stained with silver nitrate and analyzed by MS. A detailed description of the purification protocol including buffer composition is available in the Extended Experimental Procedures.

Recombinant Expression of H3K9me1 KMTs

Bacterially expressed GST-tagged Prdm16, Prdm3, Setd5, and Ash1L were purified with Glutathione Sepharose 4B resin (GE Healthcare) and eluted with PreScission protease (GE Healthcare) according to the manufacturer's protocol (GE Healthcare). Sequences of pGex6P1 expression constructs are available upon request. Eset was expressed in the Baculovirus expression system according to standard protocols (Invitrogen). FLAG-tagged Eset was purified with the M2 affinity gel (Sigma) and eluted with FLAG-peptide (Sigma) according to manufacturer's protocol (Sigma).

MS Analysis of In Vitro Methylation Products

In vitro methylation reactions with recombinant Prdm3 or Prdm16, cold SAM and histone H3 peptides (TARKST or TARK(me1)ST; 5 μM concentration) were analyzed by using nanoflow RPLC-MS on a LTQ-Orbitrap XL mass spectrometer. Peptides were identified and quantified based on high-mass accuracy/high-resolution Orbitrap FT-MS spectra. MS/MS fragmentation spectra were recorded in order to prove lysine monomethylation. A detailed description of mass spectrometric conditions and quantitative analysis is presented in the Extended Experimental Procedures.

Production of shRNAs and Lentiviral Particles

The knockdown of Prdm16, Prdm3, Eset, and Prmt5 was done by using shRNAs in a lentiviral system. Bacterial glycerol stocks of *E. coli* carrying the lentiviral plasmids were purchased from Sigma (MISSION shRNA). Plasmid DNA was transfected into 293FT cells for production of lentiviral particles according to standard protocols (RNAi consortium, Broad Institute). A detailed

cloning protocol is described in the Extended Experimental Procedures. shRNA sequences are listed in Table S4.

Immunofluorescence Staining

Wt and *Suv39h* dn iMEFs were plated on Lab-Tek II 8-well chamber slides (Nunc) and infected with respective lentiviruses. One day after infection cells were selected for puromycin resistance. Cells were fixed at days 3, 6, and 12 of knockdown with 4% paraformaldehyde and permeabilized with 0.2% Triton X-100. Immunofluorescence was performed as described before (Peters et al., 2003). Slides were evaluated in a Zeiss Axioimager Z.1 equipped with Apotomeslider and a XBO 75 Watt fluorescence bulb. Images were acquired with the 63× immersion objective and the Axiovision 4.82 software. For quantifications, an average of 300 cells was counted per staining.

Cell Lines Expressing Ectopic Prdm3, Prdm16, and Prdm16∆PR

Wt iMEFs were transfected with pCAGGS-plasmids containing Prdm3, Prdm16, or Prdm16∆PR with a C-terminal 3xFLAG-HA (F/H) tag under the control of the chicken β-actin/rabbit β-globin hybrid promoter. An IRES followed by a puromycin resistance cassette allowed for selection of stable cell lines. Plasmid sequences are available upon request.

Chromatin Immunoprecipitation

ChIP was performed according to standard protocols (Martens et al., 2005). For precipitation of F/H-tagged proteins, a mixture of anti-FLAG and anti-HA antibodies was used. Antibodies and primers are listed in Tables S3 and S5.

DNA-FISH for Major Sat Repeats

Cells were fixed with 4% PFA, extracted with 0.2% Triton X-100, and then subjected to a standard DNA-FISH protocol using a mixture of four locked DNA oligonucleotides that are complementary to the mouse major sat consensus sequence. For quantifications, an average of 300 cells was counted per staining. Sequences of the locked nucleic acid probes are listed in Table S6.

Serial Block-Face Scanning Electron Microscopy

Wt and *Suv39h* dn iMEFs were seeded on Thermanox coverslips (Nunc) and infected with the control and Prdm16/Prdm3 lentiviruses for knockdown. After 3 days of infection, cells were fixed, stained with uranyl acetate, processed according to standard EM protocols (Rouquette et al., 2009), and finally embedded in Epon resin. In order to observe the nuclei in 3D, serial block-face scanning electron microscopy (SBFSEM) was performed as previously described (Denk and Horstmann, 2004). A detailed staining and SBFSEM protocol is available in the Extended Experimental Procedures.

SUPPLEMENTAL INFORMATION

Supplemental Information includes Extended Experimental Procedures, seven figures, and six tables and can be found with this article online at http://dx.doi.org/10.1016/j.cell.2012.06.048.

REFERENCES

Aguilo, F., Avagyan, S., Labar, A., Sevilla, A., Lee, D.F., Kumar, P., Lemischka, I.R., Zhou, B.Y., and Snoeck, H.W. (2011). Prdm16 is a physiologic regulator of hematopoietic stem cells. Blood *117*, 5057–5066.

An, S., Yeo, K.J., Jeon, Y.H., and Song, J.J. (2011). Crystal structure of the human histone methyltransferase ASH1L catalytic domain and its implications for the regulatory mechanism. J. Biol. Chem. *286*, 8369–8374.

Bannister, A.J., Zegerman, P., Partridge, J.F., Miska, E.A., Thomas, J.O., Allshire, R.C., and Kouzarides, T. (2001). Selective recognition of methylated lysine 9 on histone H3 by the HP1 chromo domain. Nature *410*, 120–124.

Chuikov, S., Levi, B.P., Smith, M.L., and Morrison, S.J. (2010). Prdm16 promotes stem cell maintenance in multiple tissues, partly by regulating oxidative stress. Nat. Cell Biol. *12*, 999–1006.

Denk, W., and Horstmann, H. (2004). Serial block-face scanning electron microscopy to reconstruct three-dimensional tissue nanostructure. PLoS Biol. *2*, e329.

Dignam, J.D., Lebovitz, R.M., and Roeder, R.G. (1983). Accurate transcription initiation by RNA polymerase II in a soluble extract from isolated mammalian nuclei. Nucleic Acids Res. *11*, 1475–1489.

Dodge, J.E., Kang, Y.K., Beppu, H., Lei, H., and Li, E. (2004). Histone H3-K9 methyltransferase ESET is essential for early development. Mol. Cell. Biol. *24*, 2478–2486.

Fischle, W., Wang, Y., Jacobs, S.A., Kim, Y., Allis, C.D., and Khorasanizadeh, S. (2003). Molecular basis for the discrimination of repressive methyl-lysine marks in histone H3 by Polycomb and HP1 chromodomains. Genes Dev. *17*, 1870–1881.

Fodor, B.D., Shukeir, N., Reuter, G., and Jenuwein, T. (2010). Mammalian Su(var) genes in chromatin control. Annu. Rev. Cell Dev. Biol. *26*, 471–501.

Fritsch, L., Robin, P., Mathieu, J.R., Souidi, M., Hinaux, H., Rougeulle, C., Harel-Bellan, A., Ameyar-Zazoua, M., and Ait-Si-Ali, S. (2010). A subset of the histone H3 lysine 9 methyltransferases Suv39h1, G9a, GLP, and SETDB1 participate in a multimeric complex. Mol. Cell *37*, 46–56.

Fumasoni, I., Meani, N., Rambaldi, D., Scafetta, G., Alcalay, M., and Ciccarelli, F.D. (2007). Family expansion and gene rearrangements contributed to the functional specialization of PRDM genes in vertebrates. BMC Evol. Biol. *7*, 187.

Goyama, S., Yamamoto, G., Shimabe, M., Sato, T., Ichikawa, M., Ogawa, S., Chiba, S., and Kurokawa, M. (2008). Evi-1 is a critical regulator for hematopoietic stem cells and transformed leukemic cells. Cell Stem Cell *3*, 207–220.

Gregory, G.D., Vakoc, C.R., Rozovskaia, T., Zheng, X., Patel, S., Nakamura, T., Canaani, E., and Blobel, G.A. (2007). Mammalian ASH1L is a histone methyltransferase that occupies the transcribed region of active genes. Mol. Cell. Biol. *27*, 8466–8479.

Hayashi, K., Yoshida, K., and Matsui, Y. (2005). A histone H3 methyltransferase controls epigenetic events required for meiotic prophase. Nature *438*, 374–378.

Huang, S. (2002). Histone methyltransferases, diet nutrients and tumour suppressors. Nat. Rev. Cancer *2*, 469–476.

Huang, J., and Berger, S.L. (2008). The emerging field of dynamic lysine methylation of non-histone proteins. Curr. Opin. Genet. Dev. *18*, 152–158.

Jacob, Y., Feng, S., LeBlanc, C.A., Bernatavichute, Y.V., Stroud, H., Cokus, S., Johnson, L.M., Pellegrini, M., Jacobsen, S.E., and Michaels, S.D. (2009). ATXR5 and ATXR6 are H3K27 monomethyltransferases required for chromatin structure and gene silencing. Nat. Struct. Mol. Biol. *16*, 763–768.

Karslioglu, A.B., Perrera, V., Scaranaro, M., de la Rosa-Velazquez, I.A., van de Nobelen, S., Shukeir, N., Popow, J., Gerle, B., Opravil, S., Pagani, M., et al. (2012). A transcription factor based mechanism for mouse heterochromatin

formation. Nat. Struct. Mol. Biol., in press. Published online September 16, 2012. http://dx.doi.org/10.1038/nsmb.2382.

Kim, K.C., Geng, L., and Huang, S. (2003). Inactivation of a histone methyltransferase by mutations in human cancers. Cancer Res. 63, 7619–7623.

Kind, J., and van Steensel, B. (2010). Genome-nuclear lamina interactions and gene regulation. Curr. Opin. Cell Biol. 22, 320–325.

Lachner, M., O'Carroll, D., Rea, S., Mechtler, K., and Jenuwein, T. (2001). Methylation of histone H3 lysine 9 creates a binding site for HP1 proteins. Nature 410, 116–120.

Lan, F., and Shi, Y. (2009). Epigenetic regulation: methylation of histone and non-histone proteins. Sci. China C Life Sci. 52, 311–322.

Lehnertz, B., Ueda, Y., Derijck, A.A., Braunschweig, U., Perez-Burgos, L., Kubicek, S., Chen, T., Li, E., Jenuwein, T., and Peters, A.H. (2003). Suv39h-mediated histone H3 lysine 9 methylation directs DNA methylation to major satellite repeats at pericentric heterochromatin. Curr. Biol. 13, 1192–1200.

LeRoy, G., Orphanides, G., Lane, W.S., and Reinberg, D. (1998). Requirement of RSF and FACT for transcription of chromatin templates in vitro. Science 282, 1900–1904.

Loyola, A., Bonaldi, T., Roche, D., Imhof, A., and Almouzni, G. (2006). PTMs on H3 variants before chromatin assembly potentiate their final epigenetic state. Mol. Cell 24, 309–316.

Loyola, A., Tagami, H., Bonaldi, T., Roche, D., Quivy, J.P., Imhof, A., Nakatani, Y., Dent, S.Y., and Almouzni, G. (2009). The HP1alpha-CAF1-SetDB1-containing complex provides H3K9me1 for Suv39-mediated K9me3 in pericentric heterochromatin. EMBO Rep. 10, 769–775.

Ma, Z., Swigut, T., Valouev, A., Rada-Iglesias, A., and Wysocka, J. (2011). Sequence-specific regulator Prdm14 safeguards mouse ESCs from entering extraembryonic endoderm fates. Nat. Struct. Mol. Biol. 18, 120–127.

Martens, J.H., O'Sullivan, R.J., Braunschweig, U., Opravil, S., Radolf, M., Steinlein, P., and Jenuwein, T. (2005). The profile of repeat-associated histone lysine methylation states in the mouse epigenome. EMBO J. 24, 800–812.

McStay, B., and Grummt, I. (2008). The epigenetics of rRNA genes: from molecular to chromosome biology. Annu. Rev. Cell Dev. Biol. 24, 131–157.

Mochizuki, N., Shimizu, S., Nagasawa, T., Tanaka, H., Taniwaki, M., Yokota, J., and Morishita, K. (2000). A novel gene, MEL1, mapped to 1p36.3 is highly homologous to the MDS1/EVI1 gene and is transcriptionally activated in t(1;3)(p36;q21)-positive leukemia cells. Blood 96, 3209–3214.

Morishita, K. (2007). Leukemogenesis of the EVI1/MEL1 gene family. Int. J. Hematol. 85, 279–286.

Németh, A., and Längst, G. (2011). Genome organization in and around the nucleolus. Trends Genet. 27, 149–156.

Nishioka, K., Rice, J.C., Sarma, K., Erdjument-Bromage, H., Werner, J., Wang, Y., Chuikov, S., Valenzuela, P., Tempst, P., Steward, R., et al. (2002). PR-Set7 is a nucleosome-specific methyltransferase that modifies lysine 20 of histone H4 and is associated with silent chromatin. Mol. Cell 9, 1201–1213.

Oda, H., Okamoto, I., Murphy, N., Chu, J., Price, S.M., Shen, M.M., Torres-Padilla, M.E., Heard, E., and Reinberg, D. (2009). Monomethylation of histone H4-lysine 20 is involved in chromosome structure and stability and is essential for mouse development. Mol. Cell. Biol. 29, 2278–2295.

Ohinata, Y., Payer, B., O'Carroll, D., Ancelin, K., Ono, Y., Sano, M., Barton, S.C., Obukhanych, T., Nussenzweig, M., Tarakhovsky, A., et al. (2005). Blimp1 is a critical determinant of the germ cell lineage in mice. Nature 436, 207–213.

Okano, M., Bell, D.W., Haber, D.A., and Li, E. (1999). DNA methyltransferases Dnmt3a and Dnmt3b are essential for de novo methylation and mammalian development. Cell 99, 247–257.

Pal, S., Vishwanath, S.N., Erdjument-Bromage, H., Tempst, P., and Sif, S. (2004). Human SWI/SNF-associated PRMT5 methylates histone H3 arginine 8 and negatively regulates expression of ST7 and NM23 tumor suppressor genes. Mol. Cell. Biol. 24, 9630–9645.

Peng, J.C., and Karpen, G.H. (2007). H3K9 methylation and RNA interference regulate nucleolar organization and repeated DNA stability. Nat. Cell Biol. 9, 25–35.

Perkins, A.S., Fishel, R., Jenkins, N.A., and Copeland, N.G. (1991). Evi-1, a murine zinc finger proto-oncogene, encodes a sequence-specific DNA-binding protein. Mol. Cell. Biol. 11, 2665–2674.

Peters, A.H., O'Carroll, D., Scherthan, H., Mechtler, K., Sauer, S., Schöfer, C., Weipoltshammer, K., Pagani, M., Lachner, M., Kohlmaier, A., et al. (2001). Loss of the Suv39h histone methyltransferases impairs mammalian heterochromatin and genome stability. Cell 107, 323–337.

Peters, A.H., Kubicek, S., Mechtler, K., O'Sullivan, R.J., Derijck, A.A., Perez-Burgos, L., Kohlmaier, A., Opravil, S., Tachibana, M., Shinkai, Y., et al. (2003). Partitioning and plasticity of repressive histone methylation states in mammalian chromatin. Mol. Cell 12, 1577–1589.

Rea, S., Eisenhaber, F., O'Carroll, D., Strahl, B.D., Sun, Z.W., Schmid, M., Opravil, S., Mechtler, K., Ponting, C.P., Allis, C.D., and Jenuwein, T. (2000). Regulation of chromatin structure by site-specific histone H3 methyltransferases. Nature 406, 593–599.

Reimann, M., Lee, S., Loddenkemper, C., Dörr, J.R., Tabor, V., Aichele, P., Stein, H., Dörken, B., Jenuwein, T., and Schmitt, C.A. (2010). Tumor stroma-derived TGF-beta limits myc-driven lymphomagenesis via Suv39h1-dependent senescence. Cancer Cell 17, 262–272.

Rouquette, J., Genoud, C., Vazquez-Nin, G.H., Kraus, B., Cremer, T., and Fakan, S. (2009). Revealing the high-resolution three-dimensional network of chromatin and interchromatin space: a novel electron-microscopic approach to reconstructing nuclear architecture. Chromosome Res. 17, 801–810.

Schotta, G., Lachner, M., Sarma, K., Ebert, A., Sengupta, R., Reuter, G., Reinberg, D., and Jenuwein, T. (2004). A silencing pathway to induce H3-K9 and H4-K20 trimethylation at constitutive heterochromatin. Genes Dev. 18, 1251–1262.

Schotta, G., Sengupta, R., Kubicek, S., Malin, S., Kauer, M., Callén, E., Celeste, A., Pagani, M., Opravil, S., De La Rosa-Velazquez, I.A., et al. (2008). A chromatin-wide transition to H4K20 monomethylation impairs genome integrity and programmed DNA rearrangements in the mouse. Genes Dev. 22, 2048–2061.

Seale, P., Bjork, B., Yang, W., Kajimura, S., Chin, S., Kuang, S., Scimè, A., Devarakonda, S., Conroe, H.M., Erdjument-Bromage, H., et al. (2008). PRDM16 controls a brown fat/skeletal muscle switch. Nature 454, 961–967.

Taddei, A., Maison, C., Roche, D., and Almouzni, G. (2001). Reversible disruption of pericentric heterochromatin and centromere function by inhibiting deacetylases. Nat. Cell Biol. 3, 114–120.

Towbin, B.D., González-Aguilera, C., Sack, R., Gaidatzis, D., Kalck, V., Meister, P., Askjaer, P., and Gasser, S.M. (2012). Step-Wise Methylation of Histone H3K9 Positions Heterochromatin at the Nuclear Periphery. Cell 150, this issue, 934–947.

Towbin, B.D., Meister, P., and Gasser, S.M. (2009). The nuclear envelope—a scaffold for silencing? Curr. Opin. Genet. Dev. 19, 180–186.

Wang, H., An, W., Cao, R., Xia, L., Erdjument-Bromage, H., Chatton, B., Tempst, P., Roeder, R.G., and Zhang, Y. (2003). mAM facilitates conversion by ESET of dimethyl to trimethyl lysine 9 of histone H3 to cause transcriptional repression. Mol. Cell 12, 475–487.

Wu, H., Chen, X., Xiong, J., Li, Y., Li, H., Ding, X., Liu, S., Chen, S., Gao, S., and Zhu, B. (2011). Histone methyltransferase G9a contributes to H3K27 methylation in vivo. Cell Res. 21, 365–367.

Yamaji, M., Seki, Y., Kurimoto, K., Yabuta, Y., Yuasa, M., Shigeta, M., Yamanaka, K., Ohinata, Y., and Saitou, M. (2008). Critical function of Prdm14 for the establishment of the germ cell lineage in mice. Nat. Genet. 40, 1016–1022.

Yatsula, B., Lin, S., Read, A.J., Poholek, A., Yates, K., Yue, D., Hui, P., and Perkins, A.S. (2005). Identification of binding sites of EVI1 in mammalian cells. J. Biol. Chem. 280, 30712–30722.

Ye, Q., Callebaut, I., Pezhman, A., Courvalin, J.C., and Worman, H.J. (1997). Domain-specific interactions of human HP1-type chromodomain proteins and inner nuclear membrane protein LBR. J. Biol. Chem. 272, 14983–14989.